Nanomanufacturing of 2D Transition Metal Dichalcogenide Materials Using Self-Assembled DNA Nanotubes

*Jungwook Choi, Haorong Chen, Feiran Li, Lingming Yang, Steve S. Kim, Rajesh R. Naik, Peide D. Ye, and Jong Hyun Choi**

Atomically thin 2D films of semiconductors have emerged as promising materials for future electronics, optoelectronics, sensors, energy conversion, and storage devices.[1,2] In particular, semiconducting transition metal dichalcogenide (TMDC) materials such as MoS_2, $MoSe_2$, WS_2, and WSe_2 have received significant attention due to their unique physical properties, which depend upon the number of layers. These materials transition from an indirect bandgap in the bulk phase to an increased, direct bandgap in the monolayer, which is starkly different from other 2D materials such as zero-bandgap graphene.[3] For instance, bulk MoS_2 has an indirect bandgap of 1.2 eV, whereas monolayer MoS_2 displays a direct bandgap of 1.8 eV.[4] The monolayer MoS_2 exhibits remarkable properties including high in-plane mobility and large current on/off ratio,[5] strong photoluminescence (PL),[6] high photoresponsivity,[7] and high Young's modulus and elasticity.[8,9]

To date, most studies of TMDCs focused on investigating the synthesis and intrinsic properties of the 2D materials, and few works studied the nanofabrication of TMDCs despite their importance in future nanodevices.[10] Individual 2D monolayers of TMDCs can be effectively obtained through mechanical cleavage from bulk crystals with high crystalline quality. Other methods including liquid exfoliation,[11] lithium intercalation,[12] chemical vapor deposition,[13–15] and epitaxial growth[16,17] have been developed for scalable production and large area preparation of the TMDCs. To exploit and transfer the exceptional properties of TMDCs into diverse micro/nanodevices and systems, high-resolution nanoscale patterning of the TMDCs is critical, along with scalable and reliable production. However, large-area, parallel manufacturing of nanostructured TMDCs remains a challenge and still relies on low-throughput approaches. For example, electron beam lithography has enabled downscaling of MoS_2 transistors,[18] but its serial nature hinders the scalability in manufacturing and increases cost of fabrication. Therefore, new methods that can overcome these limitations could form a basis for rendering these 2D materials suitable in widespread applications.

Here we present a facile and generalized strategy capable of creating nanostructured TMDCs in a parallel, scalable manner. Our method combines a bottom-up self-assembly of DNA and a top-down lithographic fabrication to define 2D TMDC materials with nanogeometry. DNA self-assembly has emerged as a powerful approach for designing and organizing programmable structures of complex geometry, which may not be fabricated otherwise.[19] The in silico designs of arbitrary sizes and shapes can be transformed into 1D, 2D, and 3D nanostructures with a minimum resolution of ≈2 nm that is governed by the size of the double-helix. Such examples include smile faces,[20] multitooth gears,[21] Latin alphabet characters,[22] tubes,[23] lattices,[24] and polyhedral architectures,[25–27] to name a few. As an alternative to conventional lithography, DNA-templated nanofabrication of metallic nanowires,[28,29] inorganic nanoparticles,[30] oxide films,[31,32] and graphene[33] has also been demonstrated. Compared with widely used lithographic techniques such as electron beam[34] and dip-pen,[35] DNA self-assembly not only overcomes the limitations of serial processes but also provides high programmability and structural predictability.[31]

In this work, we demonstrate nanomanufacturing of 2D semiconducting TMDCs (MoS_2, $MoSe_2$, and WSe_2) by using self-assembled DNA nanotubes as etch masks. Two types of DNA nanotubes are assembled: one with a defined length (up to ≈300 nm) by hierarchically stacking DNA origami tubules (e.g., tubular monomers and tetramers) and the other with uncapped, double-crossover-like structures of several micrometers in length. The DNA nanotubes are deposited onto 2D planes of TMDCs and subsequently metallized with

Dr. J. Choi, H. Chen, F. Li, Prof. J. H. Choi
School of Mechanical Engineering
Purdue University
West Lafayette
IN 47907, USA
E-mail: jchoi@purdue.edu
L. Yang, Prof. P. D. Ye
School of Electrical and Computer Engineering
Birck Nanotechnology Center
Purdue University
West Lafayette
IN 47907, USA
Dr. S. S. Kim, Dr. R. R. Naik
Materials & Manufacturing Directorate
Air Force Research Laboratory
Wright-Patterson Air Force Base
OH 45433, USA

DOI: 10.1002/smll.201501431

www.MaterialsViews.com

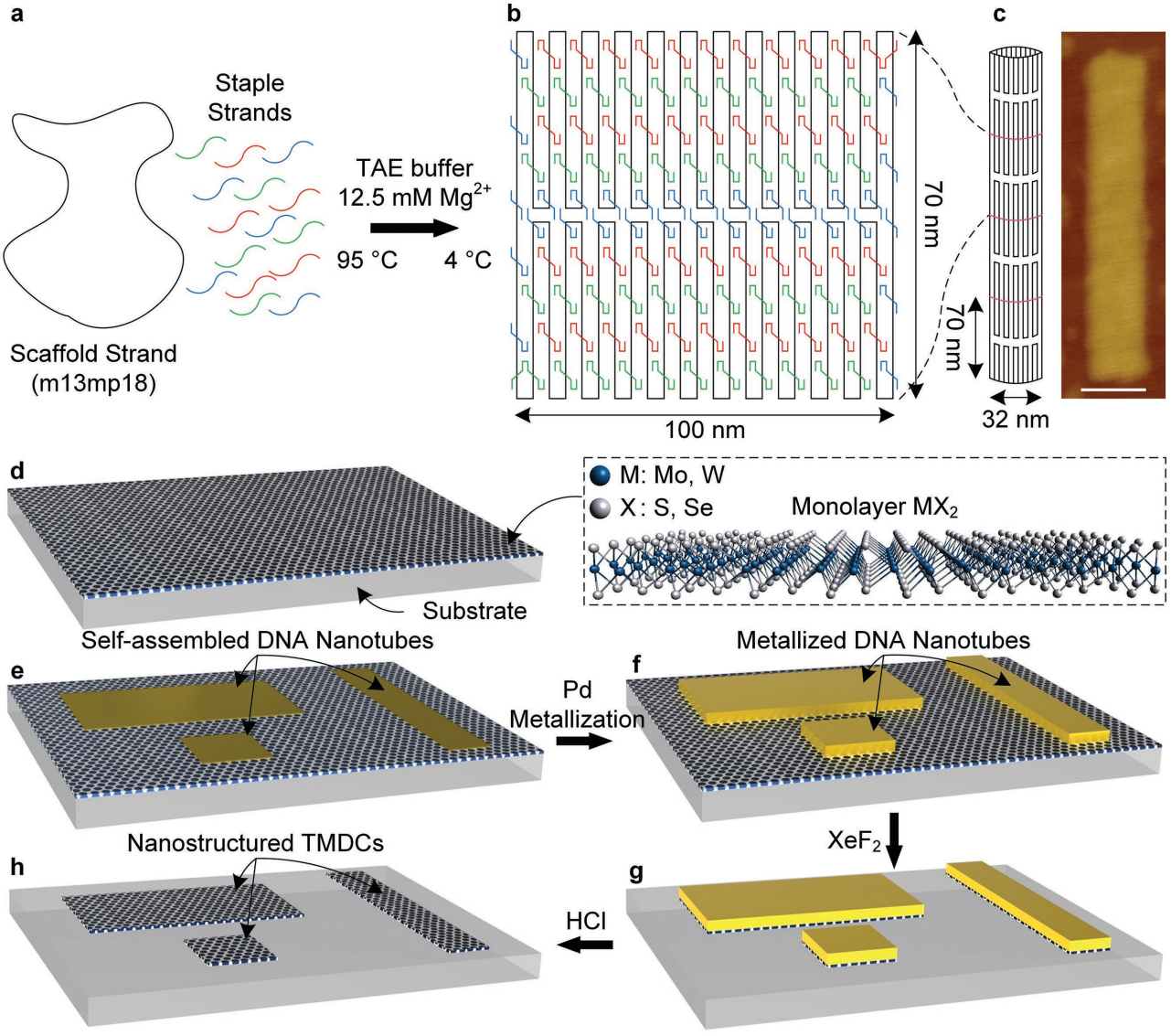

Figure 1. Nanofabrication of 2D semiconducting TMDCs using self-assembled DNA nanotubes as etch masks. a) Synthesis scheme for a DNA origami where a long-chain scaffold strand is folded with the help of staple oligonucleotides in a thermal cycler from 95 to 4 °C in TAE buffer with 12.5×10^{-3} M Mg^{2+}. b) In silico design of scaffold (black) folding pattern and staple (red, blue, and green) arrangement, forming a tubular structure of ≈32 nm in diameter and ≈70 nm in length. c) Schematic of a tetramer DNA nanotube and its AFM image. Four DNA origami tube monomers hierarchically assemble in the longitudinal direction, forming a tetramer nanotube. The nanotube is deposited onto a mica substrate and flattened to maximize its contact, measuring ≈50 nm in width and ≈280 nm in length, as expected from the design. Scale bar in the AFM image is 50 nm. d) Schematic of semiconducting TMDC materials (MX_2, where M is a transition metal such as Mo or W, and X is a chalcogen such as S or Se) exfoliated onto an SiO_2/Si substrate. e) Self-assembled DNA nanotubes are deposited on the TMDC layer. f) The DNA nanotubes are selectively metallized with Pd on the TMDCs. g) Dry etching by XeF_2 removes exposed TMDCs, whereas the area underneath the deposited DNA nanotubes is protected. h) After removal of the Pd-metallized DNA nanotubes, the nanostructured TMDCs with the designed pattern of DNA assemblies are obtained.

Pd to ensure etch selectivity against underlying TMDCs. The shapes and dimensions of the DNA nanotubes are successfully transferred onto the TMDCs, which is verified by atomic force microscopy (AFM), PL, and micro-Raman spectroscopy. A spatial mapping based on raster-scanned PL and Raman spectra verifies the optical properties and structural integrity of nanopatterned TMDCs. To the best of our knowledge, this is the first observation of PL and Raman signals from the nanostructured TMDCs which may be useful for optoelectronic nanodevices and optical nanosensors. Given that a large amount of DNA nanostructures can be easily deposited over a large area serving as etch masks, our approach offers scalability and simplicity, while minimizing process complexity, for nanomanufacturing of 2D TMDC materials.

Figure 1 illustrates our nanomanufacturing strategy for 2D TMDCs. DNA nanotubes of ≈32 nm in diameter and ≈280 nm in length were synthesized by connecting four DNA origami tubules in the axial direction (i.e., tetramer tubes). Because blunt-end association of DNA tubules cannot determine the exact length (i.e., the number of tubules), we designed two types of origami tubules with identical dimensions (e.g.,

DOI: 10.1002/smll.201501431

A and B).[36] The details of the scaffold folding and staple sequences for both types of origami tubules are provided in the Supporting Information. In each origami tubule synthesis, a long single-stranded scaffold (m13mp18; shown in black in Figure 1a,b) was folded with 194 staple oligonucleotides during a thermal ramp-down from 95 to 4 °C in 1× TAE buffer with 12.5×10^{-3} M Mg^{2+} (termed, TAEM).[37] The AFM height image in Figure 1c shows a seamlessly connected tetramer structure that is flattened to maximize its contact to the underneath substrate, measuring ≈50 nm in width and ≈280 nm in length. The height profiles indicate the thickness measures ≈4 nm, twice the thickness of a DNA duplex. Other arbitrary shapes or periodic geometries may be designed and synthesized; for examples, large-scale organization of DNA nanostructures into 2D lattices[24] could be adopted in our manufacturing process. We have used the DNA nanotubes as a proof-of-principle in this work, demonstrating that DNA assemblies can serve as lithographic templates for the TMDCs.

The self-assembled DNA nanotubes were deposited on 2D layers of MoS_2, $MoSe_2$, and WSe_2 (Figure 1d,e). 1-pyrenemethylamine was added to improve the adhesion between the DNA nanotubes and the TMDCs due to enhanced electrostatic interaction between amine group and phosphate backbone in the TAEM environment.[33] It is worth pointing out that DNA nanotubes can also be directly deposited on the TMDCs without adsorption of 1-pyrenemethylamine through van der Waals interaction with the basal plane of the TMDCs (Figure S1, Supporting Information). After deposition of the DNA nanotubes on the TMDCs, Pd-metallization on the DNA structures was performed by incubation in palladium acetate solution, followed by chemical reduction with a buffer containing sodium citrate, lactic acid, and borane dimethylamine, forming Pd-metallized nanotubes (Figure 1f).[29,38] Selective dry etching by XeF_2 removed the bare TMDCs, whereas the Pd-metallized nanotubes and the underneath TMDC area survived (Figure 1g). Finally, the Pd-DNA etch masks were removed by HCl, leaving the nanostructured TMDCs of the intended shape and dimension on the substrate (Figure 1h). We observed no significant changes in the TMDCs before and after HCl treatment (Figure S2, Supporting Information). The AFM images and height profiles measured after each fabrication step are shown in Figure S3 (Supporting Information).

The AFM images of three distinct DNA nanotubes (monomer, dimer, and tetramer) before and after metallization are shown in **Figure 2**. After monomer DNA nanotubes were synthesized (Figure 2a), the dimer or tetramer nanotubes were hierarchically assembled by connecting two or four nanotube monomers using specially designed linker strands. To precisely control the number of monomers in a DNA chain-like superstructure, two types (A and B) of the tubes were designed. Both A and B tubes have the same scaffold folding patterns and staple arrangements, and thus, exhibit identical dimensions. However, their staple sequences are distinct such that the staples do not interfere with each other, and each tube can be addressed separately (see the Supporting Information for details). A set of linkers were designed to connect the A and B nanotubes to form A–B dimers (Figure 2b). Two additional sets of linkers were used to interface the B–B and B–A nanotubes for A–B–B–A tetramer DNA nanotubes (Figure 2c). From the measurements of ten different nanotube samples (N = 10), the average lengths of monomers, dimers, and tetramers were 68.7 ± 3.5, 153.5 ± 4.8, 296.3 ± 14.8 nm, respectively (Figure 2 g–i). The average width and height of all DNA nanotubes (N = 30) were measured to be 55.6 ± 3.7 and 4.0 ± 0.3 nm, respectively.

To secure etch selectivity against underlying TMDCs, the DNA nanotubes were metallized with Pd as shown in the AFM images of Figure 2d–f. The sizes and shapes of DNA nanotubes were well preserved after metallization. Height profiles of metallized DNA nanotubes clearly indicate that the height increased twice (9.0 ± 1.3 nm, N = 27) than the as-synthesized nanotubes (Figure 2 g–i). The resolution of DNA-based TMDC nanofabrication depends on the feature size of DNA nanostructures. In our current work, the deviation in lateral dimensions before and after metallization is ≈5.3% on average. This implies that the theoretical minimum size of metallized DNA etch masks could be down to ≈2.1 nm if one uses a double-helix (≈2 nm) as a building block for nanomanufacturing. Considering the intrinsic resolution of ≈3 nm in electron beam lithography,[34] DNA nanolithography has potential for scalable nanomanufacturing, which could overcome the serial nature of electron beam, with comparable resolution.

Atomically thin TMDCs in this study were prepared by mechanical cleavage from bulk crystals on an Si substrate with a 285 nm thick oxide layer. **Figure 3** presents AFM, PL, and Raman measurements of the semiconducting monolayers MoS_2, $MoSe_2$, and WSe_2. The thicknesses of 0.9–1 nm in Figure 3a–c indicate monolayer films on the SiO_2 surface (also see Figure S4, Supporting Information). When excited at 633 nm at room temperature, the monolayers MoS_2, $MoSe_2$, and WSe_2 exhibit strong PL signatures at 660, 790, and 752 nm, respectively (Figure 3d–f).[4,12,15,39,40] This strong emission is attributed to the direct bandgap of the atomically thin semiconducting TMDCs, where the interband transition takes place at the K point of the Brillouin zone.[4] The Raman spectrum of MoS_2 in Figure 3g shows several features including first-order in-plane mode (E^1_{2g} at 386 cm^{-1}), out-of-plane mode (A_{1g} at 405 cm^{-1}), optical phonon mode (A_{2u} at 462 cm^{-1}), and second-order longitudinal acoustic mode at M point (2LA(M) at 452 cm^{-1}).[39,41,42] For $MoSe_2$, the E^1_{2g} and the A_{1g} peaks are observed at 292 and 242 cm^{-1} (Figure 3h), depending on the number of layers.[39] Thus, we conclude that the MoS_2 and $MoSe_2$ films are monolayers. The monolayer WSe_2 displays indistinguishable peak positions of the E^1_{2g} and A_{1g} modes around 250 cm^{-1},[43] as shown in Figure 3i.

The nanoscale pattern transfer from the DNA nanotubes to the MoS_2 and the $MoSe_2$ is presented in **Figure 4**. The Pd-metallized monomer DNA nanotube on the MoS_2 (N = 9) measures 9.1 ± 1.4 nm in height, 53.9 ± 3.6 nm in width, and 64.9 ± 4.9 nm in length (Figure 4a). The deviations in the width and length of the metallized DNA nanotubes, compared with their dimensions before metallization (49.8 ± 3.8 nm in width and 68.7 ± 3.5 nm in length), possibly originated from the local denaturation and/or deformation of DNA by Pd grains. After subsequent dry etching and DNA

DOI: 10.1002/smll.201501431

www.MaterialsViews.com

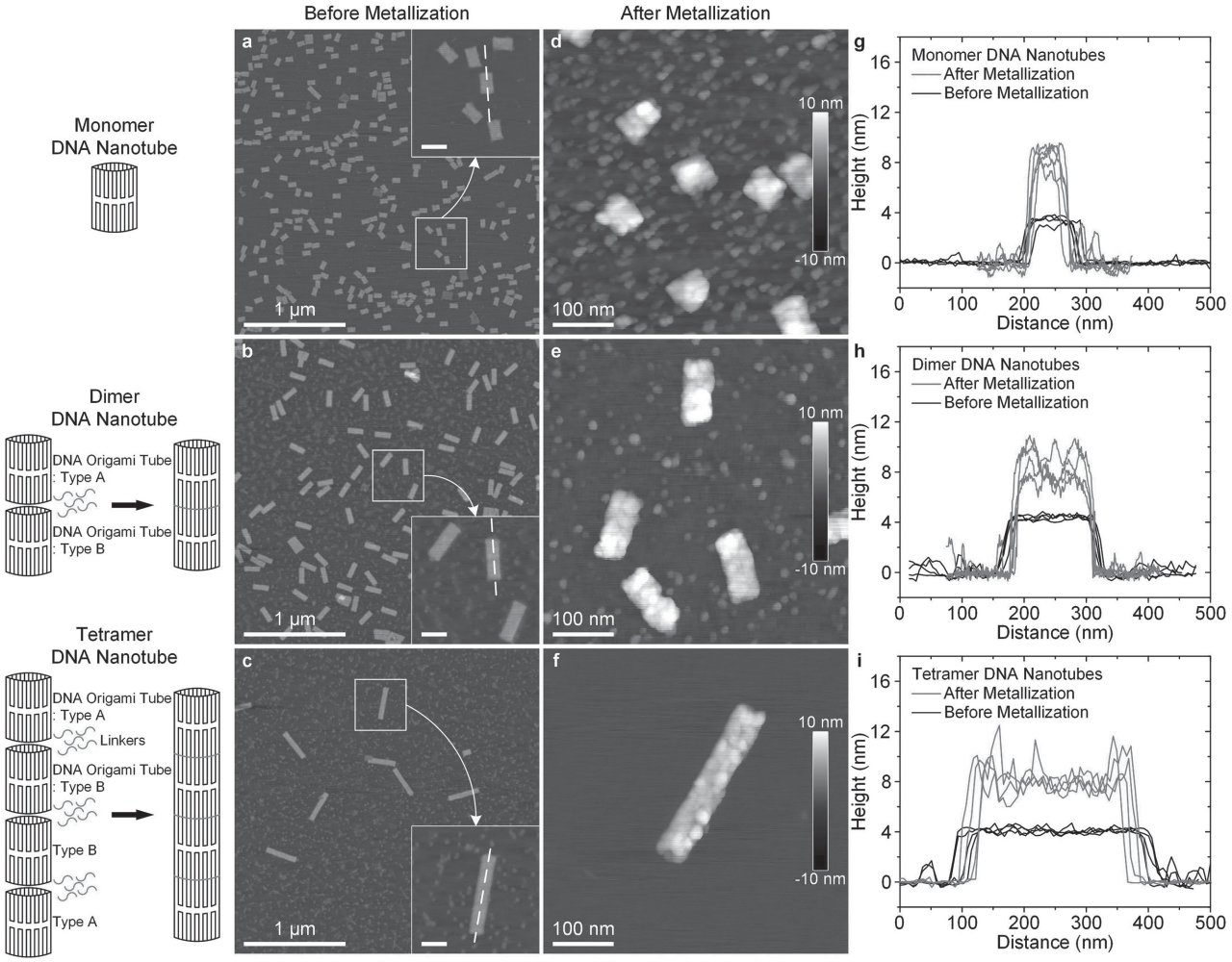

Figure 2. AFM images and height profiles of as-synthesized and metallized monomer, dimer, and tetramer DNA nanotubes. Schematics and AFM images of a) monomer, b) dimer, and c) tetramer DNA nanotubes deposited on a mica substrate. The height of DNA nanotubes is 4.0 ± 0.3 nm, twice the thickness of a DNA duplex. Two types of tubules are connected with a set of specially designed linker strands to form tube dimers (i.e., AB) or tetramers (i.e., ABBA). Insets show enlarged images and scale bars are 100 nm. AFM images of Pd-metallized d) monomer, e) dimer, and f) tetramer DNA nanotubes. Metallization increases the height of DNA nanotubes while maintaining the sizes and shapes. Height profiles of the g) monomer, h) dimer, and i) tetramer DNA nanotubes before and after metallization measured along a longitudinal direction (dotted lines in the insets of a–c). The average height of DNA nanotubes after metallization is 9.0 ± 1.3 nm.

removal, the final MoS_2 nanopattern dimensions obtained were 1.3 ± 0.2 nm in height, 49.5 ± 4.4 nm in width, and 58.1 ± 7 nm in length (N = 9), respectively (Figure 4b,c). Because the XeF_2 etching is isotropic, the resulting final dimensions shrink slightly; the shrinkage during the pattern transfer (i.e., dimensional difference between metallized DNA and patterned TMDCs) in our work is estimated to be ≈9.5%. It should be also noted that the lateral resolution of the measurements depends on the sharpness of the AFM probe tip. The precision of the pattern transfer could be improved by adopting a plasma etching with high anisotropy. Under directional plasma environment, etch selectivity of TMDCs with respect to metallized DNA should be taken into account for successful protection of underlying TMDCs. Considering the thickness difference between the monolayer TMDCs (≈1 nm) and the Pd-DNA (≈9 nm), anisotropic etch parameters such as plasma power, etching time, etchant composition, and flow rate can be optimized. To demonstrate the programmability of the DNA nanotubes and the corresponding pattern transfer to other TMDCs, the tetramer DNA nanotubes were deposited and metallized to serve as an etch mask for the $MoSe_2$ (Figure 4d,e). The dimensions of the metallized tetramer DNA nanotube measured 8.9 ± 1.4 nm in height, 68.6 ± 8.4 nm in width, and 295.6 ± 39.3 nm in length (N = 9). The final nanopatterned $MoSe_2$ had an average height, width, and length of 1.2 ± 0.1, 60.3 ± 9.7, and 285.2 ± 18.3 nm (N = 9), respectively (Figure 4f). These results demonstrate successful fabrication of the nanostructured $MoSe_2$ (also see Figure S5 in the Supporting Information for the AFM images and height profiles of the DNA nanotubes and the nanostructured MoS_2 and $MoSe_2$). Based on the statistics on the dimensions of nanostructured TMDCs, the number of the MoS_2 and the $MoSe_2$ layers corresponds to mono- and bilayer.

We extended our approach for manufacturing WSe_2 nanoribbons using a few micrometer-long DNA nanotubes. These long DNA nanotubes were synthesized using

DOI: 10.1002/smll.201501431

small NANO MICRO

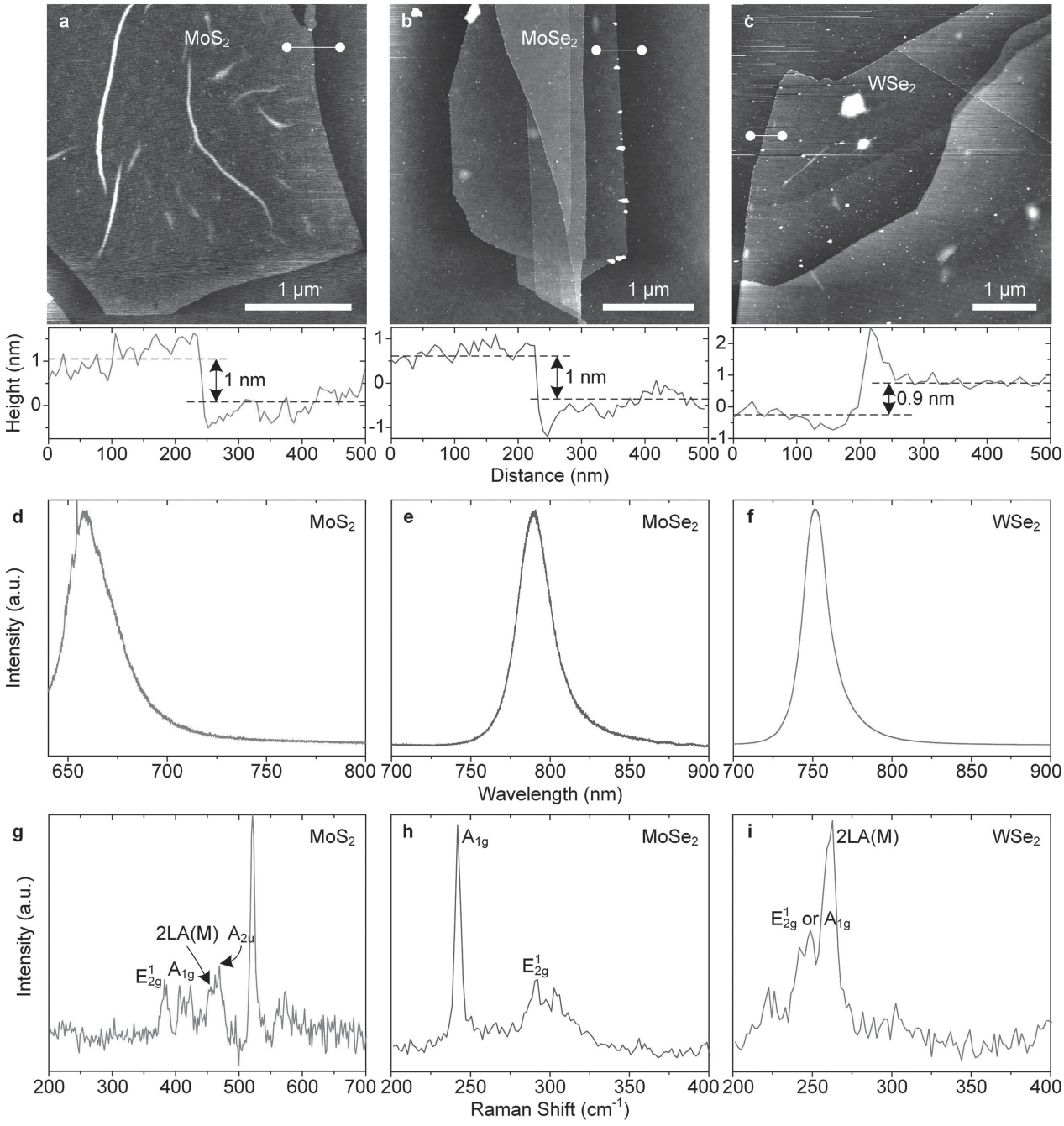

Figure 3. Optical characterization and AFM height images of semiconducting TMDCs. AFM images of mechanically exfoliated a) MoS_2, b) $MoSe_2$, and c) WSe_2 on an SiO_2/Si substrate. The presented height profiles are obtained along the white solid lines in the images. The measured thickness of 0.9–1 nm indicates TMDC monolayers. PL spectra of the d) MoS_2, e) $MoSe_2$, and f) WSe_2. The PL emission signatures of MoS_2, $MoSe_2$, and WSe_2 are centered at ≈660 nm (1.88 eV), 790 nm (1.57 eV), and 752 nm (1.65 eV), respectively. Raman spectra of the g) MoS_2, h) $MoSe_2$, and i) WSe_2. The first-order in-plane (E^1_{2g}) and out-of-plane (A_{1g}) modes are observed in all of the samples; 386 and 405 cm^{-1} for MoS_2, 292 and 242 cm^{-1} for $MoSe_2$, and 249 cm^{-1} for WSe_2. The second-order longitudinal acoustic mode (2LA(M)) is observed in MoS_2 and WSe_2 at 452 and 262 cm^{-1}, respectively. The PL and the Raman spectra in (d–i) were obtained from the MoS_2, $MoSe_2$, and WSe_2 shown in (a–c). The excitation wavelength was 633 nm for all of the spectra.

52-base-long self-complementary strands,[38] and have a width distribution from 30 to 40 nm (Figure S6 in the Supporting Information for the design and AFM measurements of these DNA nanotubes). **Figure 5**a shows a Pd-metallized DNA nanotube deposited on a WSe_2, displaying an average height of 8.5 ± 1.7 nm and width of 47.3 ± 2.1 nm. The dry etching with XeF_2 produced WSe_2 nanoribbon whose measured height and width were 2.1 ± 0.1 and 33.5 ± 3 nm, respectively (Figure 5b,c). These height and width were measured on the same metallized DNA nanotube and WSe_2 nanoribbon at five different locations. Due to the formation of Pd grain boundaries during metallization of DNA nanotubes,

DOI: 10.1002/smll.201501431

www.MaterialsViews.com

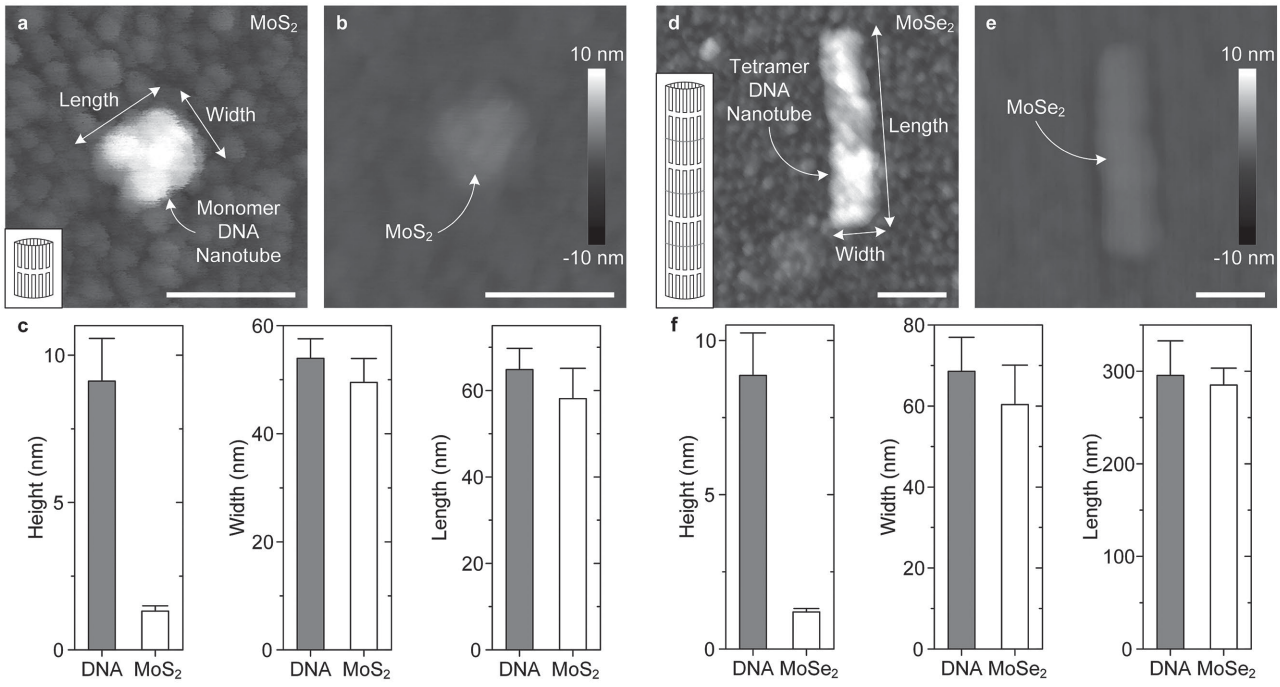

Figure 4. Nanomanufacturing of the MoS_2 and $MoSe_2$ patterns transferred from the DNA nanotubes. AFM height images of MoS_2 a) before and b) after the XeF_2 dry etching. c) Statistical distribution of the dimensions of the Pd-metallized monomer DNA nanotubes and the nanostructured MoS_2. The height, width, and length of the monomer DNA nanotubes were 9.1 ± 1.4, 53.9 ± 3.6, and 64.9 ± 4.9 nm, respectively. The resultant MoS_2 nanostructures had an average height, width, and length of 1.3 ± 0.2, 49.5 ± 4.4, and 58.1 ± 7 nm, respectively. AFM height images of d) a Pd-metallized tetramer DNA nanotube deposited on the $MoSe_2$ and e) final nanostructured $MoSe_2$. f) The height, width, and length of the tetramer DNA nanotube are 8.9 ± 1.4, 68.6 ± 8.4, and 295.6 ± 39.3 nm, respectively. The resultant $MoSe_2$ nanostructures have an average height, width, and length of 1.2 ± 0.1, 60.3 ± 9.7, and 285.2 ± 18.3 nm, respectively. Insets in (a) and (d) show the schematics of the monomer and the tetramer DNA nanotubes. Scale bars in (a,b) and (d,e) are 100 nm. The final width and length of both MoS_2 and $MoSe_2$ slightly decreased from their original designs of the DNA nanotubes due to the isotropic nature of XeF_2 etching.

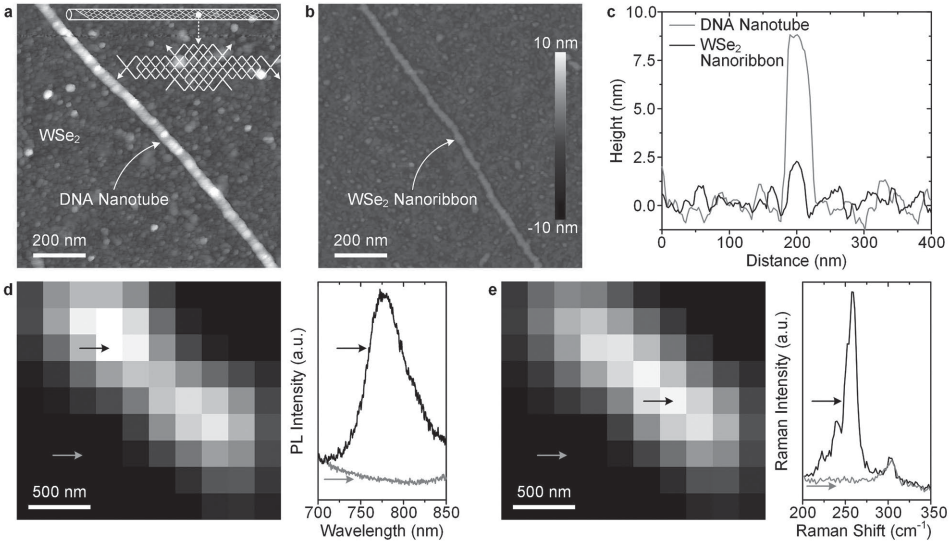

Figure 5. Patterned WSe_2 nanoribbon and optical characterization. a) AFM height image of a Pd-metallized micrometer-long DNA nanotube deposited on a WSe_2 layer. Assembly of 52-base-long self-complementary single strands forms a double-crossover-like structure (inset) with several micrometers in length. b) AFM height image of the WSe_2 nanoribbon obtained after XeF_2 etching and removal of the Pd-nanotube mask. c) Cross-sectional height profile of the DNA nanotube and the WSe_2 nanoribbon shown in (a,b). d) PL image of the WSe_2 nanoribbon reconstituted from raster-scanned PL spectra at 776 nm and the corresponding PL spectra obtained at the spots indicated by black and gray arrows. e) Raman intensity (2LA(M) peak at 259 cm^{-1}) map of the WSe_2 nanoribbon and the corresponding spectra obtained at the spots indicated by black and gray arrows. The image mapping was performed with 633 nm laser excitation at room temperature.

small 2015,
DOI: 10.1002/smll.201501431

the resulting TMDC nanoribbons could have discontinuous points and its functionality could be deteriorated after dry etching. In order to verify the functionalities of the nanopatterned TMDCs, we performed a raster-scanning of a WSe_2 nanoribbon using a confocal Raman microscope with a 100× objective lens with a laser spot size of ≈1 μm. Figure 5d,e shows the reconstructed images of the WSe_2 nanoribbon based on the recorded PL and Raman intensities at 776 nm and 259 cm^{-1}, respectively. The corresponding spectra on and off the nanoribbon are also presented. The PL and Raman imaging clearly indicates that the patterns of the DNA nanotube is well transferred to WSe_2, whereas WSe_2 in the area without the nanotube was completely removed, forming the WSe_2 nanoribbon. It is also noted that the nanoribbon in the PL and Raman images appears to have a width of ≈1 μm, which is expected given the optical diffraction limit of our measurement system. Similar observations were reported with single carbon nanotube images reconstituted based on their PL, where a 1 nm diameter nanotube appears to be ≈1 μm.[44] These results confirm that the pattern transfer from the DNA nanotube to the WSe_2 was successful without deteriorating the optical properties of the WSe_2. Our observation of the spatially resolved PL and Raman signatures is the first from the nanomanufactured TMDCs, which could be exploited for widespread applications including optoelectronic nanodevices and optical nanosensors for chemical and biological detection.

In closing, we have demonstrated the feasibility of scalable nanomanufacturing of atomically thin 2D TMDC materials using self-assembled DNA nanotubes as lithographic templates. Self-assembly of DNA nanotubes and their selective metallization enabled us to install dimension-controllable etch masks onto the TMDCs. Dry etching of the TMDCs transferred the geometrical design of the DNA nanostructures to the TMDC layers. The nanopatterned TMDCs retained strong PL and Raman signatures. Given the ability of DNA to program self-assembled structures, etch masks of arbitrary shapes and sizes can be prepared for TMDCs. Such nanostructures may be selectively metallized with various metals including Ag,[28] Au,[33] Pt,[45] and Cu.[46] Compared to traditional nanolithography techniques, the DNA-based nanofabrication offers high programmability, manufacturability, and scalability with improved spatial resolution. In addition to DNA, other self-assembled biomolecular structures such as M13 or tobacco mosaic viruses may also be explored as lithographic templates. Ultimately, our approach could be applicable to other 2D layered materials and van der Waals heterostructures for high-performance nanoelectronics and optoelectronic devices.

Experimental Section

Preparation of TMDCs: MoS_2, $MoSe_2$, and WSe_2 were mechanically exfoliated from the bulk crystals (SPI Supplies and 2D semiconductors) onto Si wafers with a 285 nm thermal oxide layer. In order to improve the adhesion between the flakes and the substrates, the surface of SiO_2 was treated with oxygen plasma for 60 s. Residues from adhesive tapes were removed by acetone and isopropyl alcohol.

Synthesis of DNA Nanotubes: Two types (A and B) of DNA origami tubules with identical dimensions were designed to form nanotubes with defined lengths: 70 nm for monomers and 280 nm for tetramers. Each set of DNA origami tubes were synthesized by a thermal ramp-down from 95 to 4 °C (1 °C per min) of 4.2×10^{-9} M m13mp18 scaffold (New England Biolabs) with 10× staple oligonucleotides in 1× TAE buffer containing 12.5×10^{-3} M magnesium acetate. The detailed design and sequence information of DNA origami tubes are presented in the Supporting Information (Figure S7). For micrometer-long DNA nanotubes, 52-mer self-complementary strands (5′-CCA AGC TTG GAC TTC AGG CCT GAA GTG GTC ATT CGA ATG ACC TGA GCG CTC A-3′) were subjected to a similar thermal treatment (95 to 4 °C over 48 h) to initiate self-assembly after purification with 20% denaturing polyacrylamide gel electrophoresis. All the oligonucleotide strands were purchased from Integrated DNA Technologies.

Deposition and Metallization of DNA Nanotubes: The mechanically exfoliated TMDCs were immersed into 0.37×10^{-3} M 1-pyrenemethylamine methanol solution for 5 min and dried by compressed air. The as-exfoliated TMDCs were also used without pre-adsorption of 1-pyrenmethylamine. Then, ≈2.5 μL of 2×10^{-9} M origami nanotubes or micrometer-long DNA nanotubes assembled from 1 μM DNA strands in 1× TAE and 12.5×10^{-3} M Mg^{2+} buffer was dropped and left for 5 min, allowing the DNA nanostructures to adsorb on the TMDCs. A drop (≈10 μL) of 11.1×10^{-3} M palladium acetate solution was subsequently added and incubated for 10 s. After drying by air, 15 μL of reducing buffer, containing 85×10^{-3} M sodium citrate, 277.5×10^{-3} M 85% lactic acid, and 42.4×10^{-3} M borane dimethylamine, was added on the TMDCs and incubated for 15 s, followed by air drying.[38] The metallized DNA-deposited TMDCs were rinsed 2–3 times with DI water or TAE buffer containing 5×10^{-3} M $MgCl_2$.

Dry Etching of TMDCs and Removal of DNA Nanotubes: The MoS_2, $MoSe_2$, and WSe_2 layers were dry etched under 3 Torr XeF_2 vapor for 5 cycles of 20 s each. The Pd metallized DNA nanotubes were then removed by immersing in 36.5%–38% HCl for 1 min and rinsed with DI water. Pd-DNA etch masks were completely dissolved by HCl, while the nanostructured TMDCs were kept intact due to their chemical inertness.

AFM and Optical Characterizations: AFM measurements were performed with a Bruker Dimension Icon and a SCANASYST-AIR probe. PL and Raman spectra were recorded at room temperature with a Renishaw inVia confocal Raman microscope using a 633 nm HeNe laser and a 100× objective lens that has ≈1 μm spot diameter. The Savitzky–Golay 25-point rolling average was used for the spectra presented in Figure 5d.

Supporting Information

Supporting Information is available from the Wiley Online Library or from the author.

Acknowledgements

The authors thank C. Mao and J. Yu for their help with synthesis of micron-sized DNA nanotubes. This work was supported by the National Science Foundation. J.H.C. also gratefully acknowledges the Air Force Summer Faculty Fellowship.

[1] D. Jariwala, V. K. Sangwan, L. J. Lauhon, T. J. Marks, M. C. Hersam, *ACS Nano* **2014**, *8*, 1102.
[2] F. Bonaccorso, L. Colombo, G. Yu, M. Stoller, V. Tozzini, A. C. Ferrari, R. S. Ruoff, V. Pellegrini, *Science* **2015**, *347*, 1246501.
[3] Q. H. Wang, K. Kalantar-Zadeh, A. Kis, J. N. Coleman, M. S. Strano, *Nat. Nanotechnol.* **2012**, *7*, 699.
[4] K. F. Mak, C. Lee, J. Hone, J. Shan, T. F. Heinz, *Phys. Rev. Lett.* **2010**, *105*, 136805.
[5] B. Radisavljevic, A. Radenovic, J. Brivio, V. Giacometti, A. Kis, *Nat. Nanotechnol.* **2011**, *6*, 147.
[6] A. Splendiani, L. Sun, Y. Zhang, T. Li, J. Kim, C.-Y. Chim, G. Galli, F. Wang, *Nano Lett.* **2010**, *10*, 1271.
[7] O. Lopez-Sanchez, D. Lembke, M. Kayci, A. Radenovic, A. Kis, *Nat. Nanotechnol.* **2013**, *8*, 497.
[8] S. Bertolazzi, J. Brivio, A. Kis, *ACS Nano* **2011**, *5*, 9703.
[9] A. Castellanos-Gomez, M. Poot, G. A. Steele, H. S. van der Zant, N. Agraït, G. Rubio-Bollinger, *Adv. Mater.* **2012**, *24*, 772.
[10] H. Nam, S. Wi, H. Rokni, M. Chen, G. Priessnitz, W. Lu, X. Liang, *ACS Nano* **2013**, *7*, 5870.
[11] J. N. Coleman, M. Lotya, A. O'Neill, S. D. Bergin, P. J. King, U. Khan, K. Young, A. Gaucher, S. De, R. J. Smith, I. V. Shvets, S. K. Arora, G. Stanton, H.-Y. Kim, K. Lee, G. T. Kim, G. S. Duesberg, T. Hallam, J. J. Boland, J. J. Wang, J. F. Donegan, J. C. Grunlan, G. Moriarty, A. Shmeliov, R. J. Nicholls, J. M. Perkins, E. M. Grieveson, K. Theuwissen, D. W. McComb, P. D. Nellist, V. Nicolosi, *Science* **2011**, *331*, 568.
[12] G. Eda, H. Yamaguchi, D. Voiry, T. Fujita, M. Chen, M. Chhowalla, *Nano Lett.* **2011**, *11*, 5111.
[13] Y.-H. Lee, X.-Q. Zhang, W. Zhang, M.-T. Chang, C.-T. Lin, K.-D. Chang, Y.-C. Yu, J. T.-W. Wang, C.-S. Chang, L.-J. Li, T.-W. Lin, *Adv. Mater.* **2012**, *24*, 2320.
[14] K.-K. Liu, W. Zhang, Y.-H. Lee, Y.-C. Lin, M.-T. Chang, C.-Y. Su, C.-S. Chang, H. Li, Y. Shi, H. Zhang, C.-S. Lai, L.-J. Li, *Nano Lett.* **2012**, *12*, 1538.
[15] J.-K. Huang, J. Pu, C.-L. Hsu, M.-H. Chiu, Z.-Y. Juang, Y.-H. Chang, W.-H. Chang, Y. Iwasa, T. Takenobu, L.-J. Li, *ACS Nano* **2014**, *8*, 923.
[16] Y. Shi, W. Zhou, A.-Y. Lu, W. Fang, Y.-H. Lee, A. L. Hsu, S. M. Kim, K. K. Kim, H. Y. Yang, L.-J. Li, J.-C. Idrobo, J. Kong, *Nano Lett.* **2012**, *12*, 2784.
[17] Q. Ji, Y. Zhang, T. Gao, Y. Zhang, D. Ma, M. Liu, Y. Chen, X. Qiao, P.-H. Tan, M. Kan, J. Feng, Q. Sun, Z. Liu, *Nano Lett.* **2013**, *13*, 3870.
[18] H. Liu, J. Gu, P. D. Ye, *IEEE Electron Device Lett.* **2012**, *33*, 1273.
[19] N. C. Seeman, *Nature* **2003**, *421*, 427.
[20] P. W. K. Rothemund, *Nature* **2006**, *440*, 297.
[21] H. Dietz, S. M. Douglas, W. M. Shih, *Science* **2009**, *325*, 725.
[22] B. Wei, M. Dai, P. Yin, *Nature* **2012**, *485*, 623.
[23] P. Yin, R. F. Hariadi, S. Sahu, H. M. T. Choi, S. H. Park, T. H. LaBean, J. H. Reif, *Science* **2008**, *321*, 824.
[24] S. Woo, P. W. K. Rothemund, *Nat. Commun.* **2014**, *5*, 4889.
[25] W. M. Shih, J. D. Quispe, G. F. Joyce, *Nature* **2004**, *427*, 618.
[26] Y. He, T. Ye, M. Su, C. Zhang, A. E. Ribbe, W. Jiang, C. Mao, *Nature* **2008**, *452*, 198.
[27] S. M. Douglas, H. Dietz, T. Liedl, B. Högberg, F. Graf, W. M. Shih, *Nature* **2009**, *459*, 414.
[28] H. Yan, S. H. Park, G. Finkelstein, J. H. Reif, T. H. LaBean, *Science* **2003**, *301*, 1882.
[29] Z. Deng, C. Mao, *Nano Lett.* **2003**, *3*, 1545.
[30] W. Sun, E. Boulais, Y. Hakobyan, W. L. Wang, A. Guan, M. Bathe, P. Yin, *Science* **2014**, *346*, 1258361.
[31] S. P. Surwade, S. Zhao, H. Liu, *J. Am. Chem. Soc.* **2011**, *133*, 11868.
[32] S. P. Surwade, F. Zhou, B. Wei, W. Sun, A. Powell, C. O'Donnell, P. Yin, H. Liu, *J. Am. Chem. Soc.* **2013**, *135*, 6778.
[33] Z. Jin, W. Sun, Y. Ke, C.-J. Shih, G. L. C. Paulus, Q. H. Wang, B. Mu, P. Yin, M. S. Strano, *Nat. Commun.* **2013**, *4*, 1663.
[34] C. Vieu, F. Carcenac, A. Pepin, Y. Chen, M. Mejias, A. Lebib, L. Manin-Ferlazzo, L. Couraud, H. Launois, *Appl. Surf. Sci.* **2000**, *164*, 111.
[35] K. Salaita, Y. Wang, C. A. Mirkin, *Nat. Nanotechnol.* **2007**, *2*, 145.
[36] H. Chen, T.-G. Cha, J. Pan, J. H. Choi, *Nanotechnology* **2013**, *24*, 435601.
[37] H. Chen, T.-W. Weng, M. M. Riccitelli, Y. Cui, J. Irudayaraj, J. H. Choi, *J. Am. Chem. Soc.* **2014**, *136*, 6995.
[38] H. Liu, Y. Chen, Y. He, A. E. Ribbe, C. Mao, *Angew. Chem., Int. Ed.* **2006**, *45*, 1942.
[39] S. Tongay, J. Zhou, C. Ataca, K. Lo, T. S. Matthews, J. Li, J. C. Grossman, J. Wu, *Nano Lett.* **2012**, *12*, 5576.
[40] C. Huang, S. Wu, A. M. Sanchez, J. J. Peters, R. Beanland, J. S. Ross, P. Rivera, W. Yao, D. H. Cobden, X. Xu, *Nat. Mater.* **2014**, *13*, 1096.
[41] B. Chakraborty, H. S. S. R. Matte, A. Sood, C. N. R. Rao, *J. Raman Spectrosc.* **2013**, *44*, 92.
[42] H. Li, Q. Zhang, C. C. R. Yap, B. K. Tay, T. H. T. Edwin, A. Olivier, D. Baillargeat, *Adv. Funct. Mater.* **2012**, *22*, 1385.
[43] E. del Corro, H. Terrones, A. Elias, C. Fantini, S. Feng, M. A. Nguyen, T. E. Mallouk, M. Terrones, M. A. Pimenta, *ACS Nano* **2014**, *8*, 9629.
[44] D. A. Tsyboulski, S. M. Bachilo, R. B. Weisman, *Nano Lett.* **2005**, *5*, 975.
[45] W. E. Ford, O. Harnack, A. Yasuda, J. M. Wessels, *Adv. Mater.* **2001**, *13*, 1793.
[46] C. F. Monson, A. T. Woolley, *Nano Lett.* **2003**, *3*, 359.

Received: May 20, 2015
Revised: July 23, 2015
Published online:

DOI: 10.1002/smll.201501431